Hydrol. Earth Syst. Sci. Discuss., 8, 9005–9062, 2011
www.hydrol-earth-syst-sci-discuss.net/8/9005/2011/
doi:10.5194/hessd-8-9005-2011

Hydrology and Earth System Sciences Discussions

Validation of SWAT simulated streamflow in the Eastern Nile and sensitivity to climate change

D. T. Mengistu[1,2] **and A. Sorteberg**[2,3]

[1]Arba Minch Institute of Technology, Arba Minch University, Ethiopia
[2]Geophysical Institute, University of Bergen, Norway
[3]Bjerknes Centre for Climate Research, University of Bergen, Norway

Received: 6 September 2011 – Accepted: 23 September 2011 – Published: 5 October 2011

Correspondence to: D. T. Mengistu (dertes_24@yahoo.com)

Published by Copernicus Publications on behalf of the European Geosciences Union.

Abstract

The hydrological model SWAT was calibrated with daily station based precipitation and temperature data for the whole Eastern Nile basin including the three subbasins: the Blue Nile, Baro Akobo and Tekeze. The daily and monthly streamflow was calibrated and validated at six outlets in the three different subbasins. The model performed very well in simulating the monthly variability of the Eastern Nile streamflow while comparison to daily data revealed a more diverse performance for the extreme events.

Of the Eastern Nile average annual rainfall it was estimated that around 60 % is lost through evaporation and estimated runoff coefficients were 0.24, 0.30 and 0.18 for Blue Nile, Baro Akobo and Tekeze subbasins, respectively. About half to two-thirds of the runoff could be attributed to surface runoff while the remaining contributions were from groundwater.

The annual streamflow sensitivity to changes in precipitation and temperature differed among the basins and the dependence of the response on the strength of the changes was not linear. On average the annual streamflow responses to a change in precipitation with no temperature change was 19 %, 17 %, and 26 % per 10 % change in precipitation while the average annual streamflow responses to a change in temperature and no precipitation change was $-4.4\,\%\,K^{-1}$, $-6.4\,\%\,K^{-1}$, and $-1.3\,\%\,K^{-1}$ for Blue Nile, Baro Akobo and Tekeze river basin, respectively.

While we show the Eastern Nile to be very sensitive to precipitation changes, using 47 temperature and precipitation scenarios from 19 AOGCMs participating in IPCC AR4 we estimated the future change in streamflow to be strongly dependent on the choice of climate model as the climate models disagree on both the strength and the direction of future precipitation changes. Thus, no clear conclusions can be made about the future changes in Eastern Nile streamflow.

HESSD

8, 9005–9062, 2011

1 Introduction

Blue Nile (Abbay), Baro Akobo (Sobat) and Tekeze (Atbara) are the three major river basins in the Eastern Nile which all originated from the Ethiopian Highlands. 86 % (or 82 km^3) of the total average flow of the Nile at Aswan is estimated to origin from these three river basins (Arsano, 2005). Several attempts have been made to implement hydrological models for Blue Nile basin. Sutcliffe et al. (1989) and Dugale et al. (1991) have used a simple daily hydrological model calibrated by METOSAT derived rainfall estimates and the National Oceanic and Atmospheric Administration, USA in collaboration with the Egyptian Ministry of Public Works has developed a comprehensive model of the Nile to predict the inflow to the Aswan Dam (Barrett et al., 1993; Schaake et al., 1993; Johanson and Curtis, 1994; Todd et al., 1995). But as Conway (1997) stated that both of these investigations suffered by the availability of in situ data, in particular subbasin discharge data to calibrate a distributed hydrological model and gauge estimates of daily rainfall to calibrate the METEOSAT derived estimates of rainfall. Conway (1997) has applied a grid-based water balance model with limited meteorological and hydrological data inputs on a monthly time step for the Blue Nile (Abbay) catchment. According to his studies (Conway, 1997), a 76-yr period the correlation between observed and simulated annual flows was 0.74 and the mean error was 14 %, although relatively large errors occurred in individual years. Using a regional atmospheric model Mohamed et al. (2005) mainly focused on the interaction between the climatic processes and the hydrological processes on the land surface over the subbasins of Nile (White Nile, Blue Nile, Atbara and the main Nile). The result showed that the model reproduces runoff reasonably well over the Blue Nile and Atbara subbasins while it overestimates the White Nile runoff (Mohamed et al., 2005). The above studies have all been investigating the upper Blue Nile (Abbay) basin but there are still very few published studies on the two other basins (Tekeze and Baro Akobo). Recently, Setegen et al. (2008) investigated the Lake Tana Basin (part of the Blue Nile) using the hydrological model (SWAT) and studies using the same model has also been conducted for the

HESSD
8, 9005–9062, 2011

Meki basin (Central Ethiopia) (Zeray et al., 2007) and the upper Awash basin (Western catchment of the Awash basin in Ethiopia) (Checkol, 2006). The above three studies showed that the model was able to describe the study areas with a quality that makes it suitable for water resource managements use.

Recently, as Fu et al. (2007) noted that several studies have investigated the sensitivity of streamflow to climate changes for basins across the world. Elshamy et al. (2009) run an ensemble of climate change scenarios using the Nile Forecasting Model with bias corrected precipitation and temperatures from 17 coupled general circulation models (AOGCMs) for the 2081–2098 period to assess the effects on the flows of the upper Blue Nile at Diem which belongs to Eastern Nile basin. From the analysis they found the upper Blue Nile to be very sensitive to precipitation (on average 30 % change in streamflow for a 10 % change in precipitation) and moderately sensitive to temperature (3.7 % change per 1 K). However the GCMs do not agree on the sign of the precipitation changes and the overall changes in total annual precipitation range from −15 % to +14 % (Elsahmy et al., 2009). As distinguished in Elshamy et al. (2009) the uncertainty in future precipitation change due to increased greenhouse gas emissions are large.

This paper aims to test the applicability of the physically based model Soil and Water Assessment Tool (SWAT) for whole Eastern Nile and thereby complementing other older studies that has simulated parts of the Eastern Nile catchment. In addition, sensitivity studies to assess the potential impacts of climate change on the annual streamflow is performed.

2 Description of the study area

The Eastern Nile and their tributaries all originate on the Ethiopian plateau and the three subbasins of the Eastern Nile lies between 5° N, 33° E and 15° N, 39° E with altitude ranges from 390 m in part of Baro Akobo (Sobat) to over 4500 m in the Tekeze (Atbara) river basin (MoWR, 2002). The total average annual flows are estimated to

HESSD
8, 9005–9062, 2011

be 50, 23.6 and 8.2 billion cubic meters from the Blue Nile (Abbay), Baro Akobo (Sobat) and Tekeze (Atbara) river basins, respectively (Arsano et al., 2004; MoWR, 2002). They provide 86 % of the waters of the Nile (Blue Nile (Abbay) 59 %, Baro-Akobo (Sobat) 14 %, Tekeze 13 %, Swain, 1997).

The Blue Nile river enters through the eastern border of Sudan from Ethiopia and flow north-west to Khartoum, where it joins the White Nile. The total length of the Blue Nile is about 940 km, and has two major tributaries, the Rahad and Dinder rivers which join downstream of Roseires (in Sudan) (Conway, 1997). Due to the high seasonal variability in rainfall over the Ethiopian plateau, the flow of the Blue Nile (Abbay) varies dramatically. The maximum runoff is in August when it is about 60 times greater than its minimum in the month of February (Arsano, 2005). The Tekeze (Atbara), rises in Northern Ethiopia Highlands and have the Angereb and Guang as its major tributaries, it replenishes the main Nile north of Khartoum. The climatic pattern and physical environment of the Tekeze subsystem are very similar to those of the Blue Nile. The Baro-Akobo (Sobat) river system marks a 380 km frontier between Ethiopia and Sudan and originates in the Western Ethiopian Highlands. Its main tributaries within Ethiopia are the Alweiro and Gilo rivers, and joins river Pibor from Sudan and rivers from Northern Uganda to form the Sobat. The Baro Akobo is the larger of the two rivers and is highly seasonal.

The climate varies from warm, desert-like climate at the Sudan border, to wet in the Ethiopian Highlands. The annual rainfall ranges from 800 mm to 2200 mm with an average of about 1420 mm for Blue Nile (Abbay). The annual rainfall reaches at maximum of 3000 mm over the highlands and a minimum of 600 mm in the lowlands with a annual rainfall of about 1419 for the case of Baro Akobo Basin. In contrast to the Blue Nile river basin (Abbay) and Baro Akobo, the annual rainfall for Tekeze (Atbara) is much lower, ranging from 600 mm to 1200 mm with an average of about 900 mm. Most of rainfall occurs from June to September for all three basins (MoWR, 2002).

HESSD
8, 9005–9062, 2011

3 Methods and materials

3.1 Model description

We use the physically based, distributed parameter model-SWAT (Soil and Water Assessment tool, version SWAT2005) which operates on daily time step and uses physiographical data such as elevation, land use and soil properties as well as meteorological data and, river discharge data for calibration (Arnold and Allen, 1996).

3.2 Hydrological processes

Hydrological processes included in the model are evapotranspiration (ET), surface runoff, infiltration, percolation, shallow and deep aquifers flow, and channel routing (Arnold et al., 1998). The effects of spatial variations in topography, land use, soil and other characteristics of watershed hydrology is incorporated by dividing a basin into several subbasins based on drainage areas of tributaries and is further divided the subbasins into a number of hydrological response unit (HRUs) within each subbasin, based on land cover and soils. Each HRU is assumed spatially uniform in terms of land use, soil, topography and climate. The subdivision of the watershed enables the model to reflect differences in evapotranspiration for various crops and soils. All model computations are performed at the HRUs level.

The fundamental hydrology of a watershed in SWAT is based on the following water balance equation (Neitsch, 2005)

$$\mathrm{SW_t} = \mathrm{SW_0} + \sum_{i=1}^{t} \left(R_{\mathrm{day}} - Q_{\mathrm{surf}} - E_{\mathrm{a}} - W_{\mathrm{seep}} - Q_{\mathrm{gw}}\right) \quad (1)$$

Where $\mathrm{SW_t}$ is the final soil water content (mm water), $\mathrm{SW_0}$ is the initial soil water content on day i (mm water), t is the time (days), R_{day} is the amount of precipitation on day i (mm water), Q_{surf} is the amount of surface runoff on day i (mm water), E_{a} is the amount of evapotranspiration on day i (mm water), W_{seep} is the amount of water

HESSD
8, 9005–9062, 2011

entering the vadose zone from the soil profile on day i (mm water), and Q_{gw} is the amount of ground flow on day i (mm water). A detail description of the different parts of the calculation is given in Appendix A.

3.3 Sensitivity of annual streamflow to climate change

The relative sensitivity of the streamflow ($\Delta Q_{\Delta P,\Delta T}$) to either a precipitation (ΔP) or a temperature (ΔT) change or a combination of the two is calculated as:

$$\Delta Q_{\Delta P,\Delta T} = \frac{\left(Q_{\Delta P,\Delta T} - Q_{\Delta P=0,\Delta T=0}\right)}{Q_{\Delta P=0,\Delta T=0}} \cdot 100 \quad (2)$$

where Q is the annual or seasonal streamflow calculated using Eq. (1).

To be able to investigate if there is any nonlinearity in the streamflow change when both precipitation and temperature are changed we estimate the linear combination of the two.

$$\Delta Q_{\Delta T,\Delta P} = a \cdot \left.\frac{\Delta Q}{\Delta P}\right|_{\Delta T=0} + b \cdot \left.\frac{\Delta Q}{\Delta T}\right|_{\Delta P=0} \quad (3)$$

where a and b are regression coefficients. Any deviation from this will indicate non-linear effects that may arise as both precipitation and temperature changed simultaneously.

3.4 Physiographical data for the three basins

A range of spatially distributed data such as topographic features, soil types, land use and the stream network (optional) are needed for the model. Table 1 summarizes the data which were processed using the AVSWAT-X interface.

HESSD
8, 9005–9062, 2011

3.4.1 Digital elevation model

A digital elevation model (DEM) was created using a 1 km^2 resolution topographic database obtained from the Ethiopian Ministry of Water Resources. The DEM (see Fig. 2) was used to delineate the watershed and the drainage patterns of the surface area analysis. Subbasin parameters such as slope gradient, slope length of the terrain, and the stream network characteristics such as channel slope, length, and width were derived from DEM.

3.4.2 Land use and soil map

Land use is one of the main factors affecting surface erosion, and evapotranspiration in a watershed. The source of land use map of the study is the Ministry of Water Resources of Ethiopia and land use/land cover map is taken from the global Hydro1K dataset (Hansen, 1998) and modified to correspond with the SWAT predefined land uses classification (Fig. 3).

More than 50 %, 23 % and 15.7 % of Blue Nile, Tekeze and Baro Akobo subbasin respectively are used for agriculture whereas the rest is covered by forest, grass, bush and shrubs. For detail see Fig. 3.

Different types of soil texture and physical-chemical properties are requirements for the SWAT model. These data were obtained from various sources. The soil map was extracted from Ministry of Water Resources of Ethiopian at Water Resources Information and Metadata Base Center department. But several properties like moisture bulk density, saturated hydraulic conductivity, percent clay content, percent silt content and percentage sand content of the soil which are required by SWAT model were not incorporated. This additional data was extracted from Wambeke (2003); USDA (1999) and FAO (1995). As seen in Fig. 4 the major soil types are lithosols and Eutric Cambisols for Tekeze sub basin: Chrome Acid Luvisols, Eutric Vertisol, Luvisols and lithic Leptosols for Blue Nile and Dystric cambisols and orthic Acrisols for Baro Akobo subbasin.

HESSD
8, 9005–9062, 2011

3.4.3 Meteorological data

SWAT requires daily meteorological data which were obtained from the Ethiopian National Meteorological Agency (NMSA) for the period 1987–2006. Figure 5 shows the stations used in this study and Table 2 summarize the number of stations in each subbasin. Missing values were filled using the SWAT built-in weather generator developed by Nicks (1974). The precipitation generator uses a first-order Markov chain model. For each subbasin input to the weather generator was observed precipitation data for the weather station that was nearest the centroid of the subbasin and having a record length from 1967–2006. Given the observed wet and dry days frequencies, the model determine stochastically if precipitation occurs or not. When a precipitation event occurs, the amount is determined by generating values from a skewed normal daily precipitation distribution or a modified exponential distribution which is calculated based on the observed data. The amount of daily precipitation is partitioned between rainfall and snowfall using average daily air temperature. The average percentage of missing data in the observed datasets is less than 10 % and 5 % of precipitation and temperature recorded data set, respectively.

3.4.4 River discharge

Stream gauged discharge data were collected from the Ministry of Water Resources of Ethiopia. Table 3 summarizes the number of stream gauges with the date of the record length used for calibration and validation. All the flow data were daily except at Diem (Blue Nile, Sudan Border) where only monthly data was available.

3.5 Sensitivity analysis

After pre-processing of the data and SWAT model set up, simulation was done for the period indicated in Table 3 for the three subbasins. The built-in SWAT sensitivity analysis tool that uses the Latin Hypercube One-factor-AT-a-Time (LH-OAT) (Griensven

HESSD
8, 9005–9062, 2011

et al., 2002, 2005) was used. Six outlets (Fig. 1) were selected for the sensitivity analysis; Three of them (Tana outlet, Kessie and Diem) in the Blue Nile, and two in Baro Akobo (Gambella and Pilog) and one in Tekeze (Embamadre).

According to Lenhart et al. (2002) the sensitivity of a flow to a parameter can be categorized into four classes. If the relative sensitivity lies between 0–0.05 and 0.05–0.2, then the parameter are classified as negligible and medium, respectively, whereas if it is varying between 0.2–1.0 and greater than 1 then categorized as high and very high class, respectively. Out of 28 selected parameters the curve number (Eq. A8), available water capacity (Eq. 1), average slope steepness, saturated hydraulic conductivity (Eq. A35), soil evaporation compensation factor (Eq. A29), soil depth, maximum canopy storage (Eq. A15), threshold water depth in the shallow aquifer for flow (Eq. A34), and base flow alpha factor (Eq. A40) was identified as being parameters to which the flow has medium, high or very high sensitivity. The ranking of the parameters were different at various outlets where sensitivity test was carried out. However the curve number (CN_2) was the main sensitivity parameter for all outlets. As it is discussed in the appendix A about the CN_2, the curve number depends on several factors including soil types, soil textures, soil permeability, land use properties etc. In addition, the relative sensitivity of the available water capacity, the soil evaporation compensation factor and the saturated hydraulic conductivity was high in all outlets. From the sensitivity test, eight parameters having a relative sensitivity greater than 0.05 (sensitivity of the flow to the parameter categorized as medium or higher) was selected for the calibration process.

3.5.1 Calibration and verification

Watershed models contain many parameters; these parameters are classified into two groups: physical and process parameters. A physical parameter represents physically measurable properties of the watershed (e.g. areas of the catchment, fraction of impervious area and surface area of water bodies, surface slope etc.) while process parameters represents properties of the watershed which are not directly measurable e.g.

HESSD
8, 9005–9062, 2011

average or effective depth of surface soil moisture storage, the effective lateral inflow rate, the coefficient of non linearity controlling the rate of percolation to the groundwater (Sorooshian and Gupta, 1995). Thus, calibrations against available streamflow observations are often conducted to tune the model. Because automatic calibration relies heavily on the optimization algorithm and the specified objective function we follow the recommendations of Gan (1988) to use both manual and automatic calibration procedures. We first conducted manual calibration of daily stream using the procedure developed by Santhi et al. (2001) (see Appendix B). Parameters identified from the sensitivity analysis were varied in sequence of their relative sensitivity within their ranges (Table 4) until the volume is adjusted to the required quantity (Zeray et al., 2007). This process continued till the volume simulated is within ±15 % of the gauged volume. The surface runoff adjustment was then followed by that of the baseflow. Here,the same apporach was followed being the adjustment made to the most sensitivity parameters affecting the base flow. Each time the baseflow calibration is finalized, the surface runoff volume was also checked as adjustment of the baseflow parameters can also affect the surface runoff volume. The same procedure was followed to calibrate the water balance of the monthly flows. After each calibartion, the coefficient of determintation (R^2) and Nash–Sutcliffe efficieny value (E_N) were checked ($R^2 > 0.6$ and $E_N > 0.5$, Santhi et al., 2001). Finally, the automatic calibration algorithm in SWAT is used for fine tuning the calibration. This is based on the Shuffled Complex Evolution algorithm developed at the University of Arizona (SCE-UA) which is a global search algorithm that minimizes a single objective function for up to 16 model parameters (Duan et al., 1992).

4 Results and discussion

4.1 Model calibration and verification

The performance of SWAT was evaluated using the Nash–Sutcliffe efficiency value (E_N) and the coefficient of determination (proportion of the variance in the observations

HESSD
8, 9005–9062, 2011

explained by the model, R^2). The difference between the E_N and the R^2 is that the E_N can interpret the model performance in the replicating individually observed values while the R^2 does not (Rossi et al., 2008). It is only measuring the deviation from the best fit line. In addition the percentage difference (PBias) indicating the systematic difference between the model and observations and the ratio of the root mean square error between simulated and observed values to the standard deviation of the observations (RSR) was used. The equations and the interpretation of the values are given in Table 5. After manual and automatic calibration the daily, monthly and annual streamflow was compared against the observed data.

4.1.1 Blue Nile calibration and verification

The model was calibrated for the Blue Nile with one upstream (Tana), one mid-way (Kessie) and one downstream (at the Sudan Border) station. The model slightly overestimates the flow in the upper and middle part of the basin and underestimates it in the lower part (Table 6) during the calibration period (the calibration and verification periods are given in Table 3). The overestimation is particularly pronounced during extreme events (not shown). There was good agreement between simulated and observed flow variability on both daily and monthly time scale for the subbasins (Fig. 7a) for most of the years except 1995, when little rainfall was recorded at Tana outlet. The E_N and R^2 ranged from 0.62 to 0.90 and 0.90 to 0.97, respectively for the monthly calibration (see Table 7 for further details). The daily calibration statistics were lower ranging from 0.62 to 0.65 and 0.77 for E_N and R^2, respectively (see Table 6).

HESSD
8, 9005–9062, 2011

In the validation period, the simulated over-estimate the flow at Tana outlet and at Kessie for the year 2000 giving slightly higher bias than in the verification period. The daily and monthly E_N simulation efficiency is between 0.53 and 0.65 and 0.55 to 0.57, respectively.

4.1.2 Baro Akobo calibration and verification

During both calibration and verification, the daily and monthly observed and simulated flows show a very good agreement (Figs. 6a and 7b). For daily data the Nash–Sutcliffe efficiency value (ENs) ranged from 0.70 to 0.81 for the calibration period and was 0.64 for the verification period (Table 6). The monthly values was higher than 0.80 for both periods. A mean deviation of 1 % shows a good agreement between measured and simulated monthly flows, respectively (Table 7). As shown in Figs. 6a and 7b the model slightly under estimated peak flows in most of the calibration periods for both daily and monthly flow.

4.1.3 Tekeze calibration and verification

Calibration and validation of the Tekeze flow near Embamadre shows a E_N of 0.8 and 0.5 for monthly and daily values during the calibration period, with a R^2 of 0.81 and 0.60 (Tables 7 and 6), respectively. A bias of 2 % in the calibration period indicates a good agreement between measured and simulated monthly flows (Table 7).

4.2 The annual water balance of the Eastern Nile

Table 8 illustrates the average annual water balance during calibration and verification of the Eastern Nile Basin for the entire calibration and validation periods. 58/57 %, 56/58 % and 62/64 % of the average annual rainfall is lost through evaporation in Blue Nile, Baro Akobo and Tekeze subbasin of the Eastern Nile during calibration and validation, respectively. The results give an average runoff coefficient of 0.24, 0.30 and 0.18

HESSD
8, 9005–9062, 2011

for Blue Nile, Baro Akobo and Tekeze subasins, respectively. Surface runoff carries 55/58.5 %, 71.6/74 % and 51/54 % of the water yield during the calibration and validation process for Blue Nile, Baro Akobo and Tekeze subbasins, respectively. Whereas the groundwater contribution is 46/43 % for Blue Nile, 31.7/30 % for Baro Akobo and 50/47 % for Tekeze during calibration and validation period, respectively.

4.3 Sensitivity of annual Eastern Nile streamflow to climate change

The sensitivity of streamflow to climate change was investigated by using several hypothetical scenarios imposed on the 1991–2000 meteorological data. Incremental climate change scenarios were applied with a hypothetical temperature increase (0, +2 and +4 °C) and a change in precipitation (−20 %, −10 %, −5 %, 0 %, +5, +10 % and +20 %) to examine the sensitivity of the SWAT streamflow to the meteorological parameters.

4.3.1 Sensitivity to precipitation changes

Sensitivity of annual streamflow to changes in precipitation, holding the temperatures fixed (Eq. 2) is different among the three subbasins. As a first approximation a linear regression analysis of the streamflow responses for the various scenarios indicates that a 10 % change in precipitation will produce a 19 %, 17 %, and 26 % change in stream flow for Blue Nile, Baro Akobo and Tekeze river basin, respectively (Fig. 8). Table 9 shows that the Blue Nile is equally sensitive to a reduction and increase in precipitation and the sensitivity is changing linearly with the precipitation change. This is not the case for Tekeze. The sensitivity to a precipitation increase is larger than to a decrease in precipitation (−42 % and 63 % change for a −20 % and +20 % precipitation changes, respectively). For Baro Akobo subbasin this is the opposite. Sensitivity is stronger to a decline in precipitation (−38 % and 29 % for −20 and +20 % precipitation change, respectively). The change in sensitivity is likely due to the difference in topography and catchment characteristics of the subbasins. In the case of Tekeze basin most

HESSD
8, 9005–9062, 2011

of the regions are categorized with a gentle slope, where sheet flow is dominating during an increase in precipitation. This is in contrast to Baro Akobo where 2/3 of the total drainage area is a plain. The land use and soil type of the two basins are also quite different. The depth of soil in the Tekeze subbasin is shallower than Baro Akobo. So, with an increase in precipitation, the response of the catchment generating direct streamflow will be smaller since more water is infiltrated down to recharge the groundwater in the case of Baro Akobo subbasin. Thus, the sensitivity of Baro Akobo to an increase in precipitation will be smaller.

4.3.2 Sensitivity to temperature change

The relative sensitivity of streamflow to changes in temperature, holding the precipitation fixed (Eq. 2) is modest in all three subbasins (Fig. 9). A linear regression analysis of the streamflow responses for the various temperature scenarios indicates that a 1 °C increase in temperature will produce a 4.4 %, 6.4 %, and 1.3 % reduction in streamflow for Blue Nile, Baro Akobo and Tekeze river basin, respectively (Fig. 9). However, the sensitivity is not linear. Two of the subbasins (Blue Nile and Baro Akobo) show a large sensitivity from 0 to +2 °C than from +2 °C to +4 °C. The reason is mainly due to the evaporation losses from the soil. When the temperature rises, the available water at the top surface of the soil gets lost easily whereas it is difficult to evaporate water from the deeper layers of the soil. Thus, a small change in temperature dries out the upper soil layer while a larger change will be less efficient in changing evaporation as the upper soil is already tried out. The Tekeze basin is less sensitive to temperature change compared to the other basins because the basin has limited moisture for approximately 2/3 of the year with today's temperatures.

4.3.3 Combined effect of temperature and precipitation on annual streamflow

Comparing the relative sensitivity of the streamflow when both temperature and precipitation is changed with the linear combination of separate temperature and precipitation

HESSD
8, 9005–9062, 2011

changes (Eq. 3), reveals that two of the subbasins show sensitivity that is not a linear function of the temperature and precipitation change (Fig. 10). Baro Akobo (Fig. 10a) shows a stronger response to a combined temperature increase and precipitation decrease than to a temperature and precipitation increase. As an example a 2 °C temperature increase and a 20 % precipitation decrease gives a streamflow reduction of 43 % while a similar temperature increased combined with a 20 % precipitation increase increases the flow with only 22 %. Interestingly, the Tekeze subbasin response is opposite. Here a 2 °C temperature increase and a 20 % precipitation decrease gives a streamflow reduction of 41 % while a similar temperature increased and a 20 % precipitation increase increases the flow with 64 %.

Compared to the other two basins the Blue Nile subbasin shows a response that is closer to the combination of a linear temperature and precipitation response.

4.3.4 Estimation of future streamflow using IPCC AR4 simulations

Using the CMIP3 global coupled climate models (AOGCMs) to calculate annual mean temperature and precipitation changes from 1980–2000 to 2080–2100 for the three subbasins using three different emission scenarios (SRES A2, A1B and B1) and 19 models (a total of 47 simulations for each basin) revealed that models all agree on a temperature rise, but disagree on the direction of precipitation change (Fig. 11). As the AOGCMs often have large biases when it comes to reproducing the regional climatic features they are not well suited to force hydrological models without extensive bias corrections. An alternative to this is to use the combined temperature-precipitation sensitivities ($\Delta Q_{\Delta P,\Delta T}$) reported above and linearly interpolate the results to the temperature and precipitation changes of the AOGCMs. It is clear that the large uncertainty in the models precipitation change is translated into large uncertainties in the streamflow changes (Fig. 12). Around 60 %, 40 % and 55 % of the estimates indicate an increased annual flow in the Blue Nile, Baro Akobo and Tekeze, respectively and the ensemble mean changes are modest in all three basins (5 %, −1 %, and 12 % the Blue Nile, Baro Akobo and Tekeze, respectively). However, the extremes ranges from a 152 % increase

HESSD
8, 9005–9062, 2011

in the Tekeze basin using the CCSM 3.0 SRES A2 scenario changes to a 55 % reduction in the same basin using the same scenario, but the GFDL CM2.0 values (Fig. 12c). A large spread in the streamflow changes was also noted by Elshamy et al. (2009).

5 Summary and conclusion

This study report on a first attempt to use a physically based, distributed hydrological model forced with daily station based precipitation and temperature data and calibrated with daily streamflow measurements to simulate the whole Eastern Nile basin.

SWAT2005 adequately simulated monthly variability in flows for the Eastern Nile basin. The total simulated monthly streamflow range from good ($0.65 < E_N < 0.75$ to very good ($E_N > 0.75$). The average daily and monthly difference between the observed and simulated flow (PBIAS) was good (PBIAS $\leq \pm 20$ %) for the calibration period with the exception of the Blue Nile subbasin were it was only satisfactory (± 20 % < PBIAS $\leq \pm 40$ %). In summary, good performance of the model in the validation period indicates that the fitted parameters during calibration period listed in Table 4 can be taken as a representative set of parameters for Eastern Nile watershed and further simulation and evaluation of alternative scenario analysis can be carried out for other periods using the SWAT model. The model simulates monthly flows better than daily flows and the model is probably not adequate for studies of single sever events in small catchments.

Of the Eastern Nile average annual rainfall it was estimated that around 60 % is lost through evaporation. The simulations estimated the runoff coefficients to be 0.24, 0.30 and 0.18 for Blue Nile, Baro Akobo and Tekeze subasins, respectively. Surface runoff carries around 55 % of the streamflow in the Blue Nile and Tekeze while in Baro Akobo the percentage is around 72. The remaining contribution is from groundwater.

The streamflow sensitivity to changes in precipitation and temperature differed among the basins and depended on the strength of the changes. The annual streamflow responses to a 10 % change in precipitation with no temperature change was on

HESSD
8, 9005–9062, 2011

average 19 %, 17 %, and 26 % for Blue Nile, Baro Akobo and Tekeze river basin, respectively. However, the response to a reduction and increase in precipitation was not the same. While Baro Akobo was more sensitive to a reduction in precipitation, Tekeze showed a larger sensitivity to an increase.

The streamflow sensitivity to temperature was relatively low. The average annual streamflow responses to a 1 °C change in temperature and no precipitation change was −4.4 %, −6.4 %, and −1.3 % for the Blue Nile, Baro Akobo and Tekeze river basin, respectively. The very low sensitivity of the Tekeze basin indicates that flow is moisture limited for a large part of the year.

The general assessment, which is made by a relative sensitivity analysis for the 20 hypothetical climate change scenarios, is that the Eastern Nile annual streamflow is very sensitive to variations in precipitation and moderately sensitive to temperature changes.

Using the combined temperature-precipitation sensitivities and 47 temperature and precipitation scenarios from 19 AOGCMs participating in IPCC AR4 we estimated the streamflow change to vary strongly as the climate models disagree on both the strength and the direction of future precipitation changes making it difficult to say anything about the future changes in Eastern Nile streamflow. This uncertainty may have implications for long term water resource planning, estimation of the future hydropower potential, reservoir design and to which extent development of agriculture should utilize river or groundwater based irrigation systems.

Finally we note that a weakness of this analysis is that it tries to address the climate change impact with only one hydrological model and two forcing variables (precipitation and temperature), neglecting all other variables (such as vegetation or radiation changes) which may affect the runoff generation. In our sensitivity studies we have multiplied the precipitation with a fraction. This means that we assume that the wet-day frequency is unchanged and the whole precipitation change is given as a change in intensity. For temperature we have added a constant for the whole year and thereby assuming that the change is not depending on season. These are all crude assumptions,

HESSD
8, 9005–9062, 2011

but given the uncertainties in future precipitation and temperature changes in the regions we feel that these simplifications are justified with our current knowledge.

Appendix A

Major hydrological processes calculated in SWAT

A1 Surface runoff

Surface runoff occurs whenever the rate of water application to the ground surface exceeds the rate of infiltration. When water is initially applied to a dry soil, the application rate and infiltration rates may be similar. However, the infiltration rate will decrease as the soil becomes wetter. When the application rate is higher than the infiltration rate, surface depressions begin to fill. If the application rate continues to be higher than the infiltration rate once all surface depressions have filled, surface runoff will start.

SWAT offers two methods for estimating surface runoff: the SCS (Soil conservation service) curve number procedure (USDA-SCS, 1972) and the Green and Ampt infiltration method (Green and Ampt, 1911). In this study, the SCS curve number method was used to estimate surface runoff volumes due to the unavailability of sub daily rainfall data needed for the Green and Ampt method. The SCS runoff equation is an empirical equation that came into use in the 1950s (Guo et al., 2008). Curve number has been calibrated and evaluated for many sets of measured runoff data and is known to be generally reliable over a wide range of geographic, soil, and land management conditions (USDA-SCS, 1985). The curve number method estimates a runoff depth, Q (mm), and a storage term, S, which is a function of the curve number, CN. Curve Numbers are assigned based on soil type (hydrologic soil group) and land use, and are modified depending on soil moisture content at the time of rainfall (Ponce and Hawkins, 1996):

HESSD
8, 9005–9062, 2011

$$Q_{\text{surf}} = \frac{(R_{\text{day}} - I_{\text{a}})^2}{(R_{\text{day}} - I_{\text{a}} + S)} \quad \text{(A1)}$$

where Q_{surf} is the accumulated runoff or rainfall excess (mm), R_{day} is the rainfall depth for the day (mm), I_{a} is the initial abstraction which includes surface storage, interception and infiltration prior to runoff (mm), and S is the retention parameter (mm). The retention parameter varies spatially due to changes in soils, land use, management and slope and temporally due to changes in soil water content. The retention parameter is defined as:

$$S = 25.4\left(\frac{1000}{\text{CN}} - 10\right) \quad \text{(A2)}$$

where CN is the curve number for the day. The initial abstractions, I_{a}, is commonly approximated as $0.2S$ and Eq. (A1) becomes

$$Q_{\text{surf}} = \frac{(R_{\text{day}} - 0.2S)^2}{(R_{\text{day}} + 0.8S)} \quad \text{(A3)}$$

Runoff will only occur when $R_{\text{day}} > I_{\text{a}} (= 0.2S)$. The retention parameter varies with soil profile water content according to the following equation:

$$S = S_{\text{max}} \cdot \left(1 - \frac{\text{SW}}{[\text{SW} + \exp(w_1 - w_2 \text{SW})]}\right) \quad \text{(A4)}$$

where S is the retention parameter for a given moisture content (mm), S_{max} is the maximum value the retention parameter can achieve on any given day (mm), SW is the soil water content of the entire soil profile excluding the amount of water held in the profile at wilting point (mm of water), and w_1 and w_2 are shape coefficients.

The maximum retention parameter value, S_{max}, is calculated by solving Eq. (A2) using CN_1.

$$S_{\text{max}} = 25.4\left(\frac{1000}{\text{CN}_1} - 10\right) \quad \text{(A5)}$$

HESSD
8, 9005–9062, 2011

Where CN_1 is moisture condition I which is the lowest value that the daily curve number can assume in dry (wilting point) condition

The shape coefficients are determined by solving Eq. (A4) assuming that

1. the retention parameter for moisture condition I curve number corresponds to wilting point soil profile water content,
2. the retention parameter for moisture condition III curve number corresponds to field capacity soil profile water content, and
3. the soil has a curve number 99 ($S = 2.54$) when it is completely saturated.

$$w_1 = \ln\left[\frac{\mathrm{FC}}{1 - S_3 \cdot S_{\max}^{-1}} - \mathrm{FC}\right] + w_2 \cdot \mathrm{FC} \tag{A6}$$

$$w_2 = \frac{\left(\ln\left[\frac{\mathrm{FC}}{1-S_3 \cdot S_{\max}^{-1}} - \mathrm{FC}\right] - \ln\left[\frac{\mathrm{SAT}}{1-2.54 \cdot S_{\max}^{-1}} - \mathrm{SAT}\right]\right)}{(\mathrm{SAT} - \mathrm{FC})} \tag{A7}$$

where w_1 is the first shape coefficient, w_2 is the second shape coefficient, FC is the amount of water in the soil profile at field capacity (mm of water), S_3 is the retention parameter for the moisture condition III curve number, $S_{\max}$ is the retention parameter for the moisture condition I curve number, SAT is the amount of water in the soil profile when completely saturated (mm of water), and 2.54 is the retention parameter value at saturation (CN = 99).

The daily curve number value adjusted for moisture content is calculated by rearranging Eq. (A2) and inserting the retention parameter calculated for that moisture content:

$$\mathrm{CN} = \frac{25\,400}{(S + 254)} \tag{A8}$$

HESSD
8, 9005–9062, 2011

Where CN is the curve number on a given day and S is the retention parameter calculated for the moisture content of the soil on that day Eq. (A4).

The moisture condition II and III curve numbers are calculated from Eqs. (A9) and (A10).

$$CN_1 = CN_2 - \frac{20 \cdot (100 - CN_2)}{(100 - CN_2 + \exp[2.533 - 0.0636 \cdot (100 - CN_2)])} \quad \text{(A9)}$$

$$CN_3 = CN_2 \cdot \exp[0.00673 \cdot (100 - CN_2)] \quad \text{(A10)}$$

Where CN_2 is moisture condition II which is the average value that the daily curve number can assume in average moisture condition and CN_3 is moisture condition III that the daily curve number can assume in wet moisture (field capacity) condition.

The moisture condition II curve number provided in the tables of SWAT manual are assumed to be appropriate for 5 % slopes. Williams (1995) developed an equation to adjust the curve number to a different slope:

$$CN_{2S} = \frac{(CN_3 - CN_2)}{3} \cdot [1 - 2 \cdot \exp(-13.86 \cdot slp)] + CN_2 \quad \text{(A11)}$$

Where CN_{2S} is the moisture condition II curve number adjusted for slope, CN_3 is the moisture condition III curve number for the default 5 % slope, CN_2 is the moisture condition II curve number for the default 5 % slope, and slp is the average percent slope of the subbasin.

The flow is then predicted separately for each HRU and routed to obtain the total runoff for the watershed. This increases accuracy and gives a much better physical description of the water balance (Arnold et al., 1998).

A2 Evapotranspiration

An accurate estimation of evapotranspiration is critical in the assessment of water resources and the impact of climate and land use change.

HESSD
8, 9005–9062, 2011

Among the three methods (the Penman–Monteith method, Monteith, 1965; Allen et al., 1986), the Priestley–Taylor method (Priestley and Taylor, 1972) and the Hargreaves method (Hargreaves et al., 1985) incorporated in SWAT, we use the Hargreaves method to estimate potential evapotraspiration. The method was selected due to the fact that it requires only air temperature. The form used in SWAT was published is (Hargreaves et al., 1985);

$$\lambda E_0 = 0.0023 H_0 (T_{mx} - T_{mn})^{0.5} \cdot \left(\overline{T}_{\text{av}} + 17.8\right) \tag{A12}$$

Once total potential evapotranspiration is determined, actual evaporation must be calculated. SWAT first evaporates any rainfall intercepted by the plant canopy. Next, SWAT calculates the maximum amount of transpiration and the maximum amount of sublimation/soil evaporation using an approach similar to that of Ritchie (1972). The actual amount of sublimation and evaporation from the soil is then calculated.

A2.1 Evaporation of intercepted Rainfall

The amount of actual evapotranspiration contributed by intercepted rainfall is especially significant in forests where in some instances evaporation of intercepted rainfall is greater than transpiration.

SWAT removes as much water as possible from canopy storage when calculating actual evaporation. If potential evapotranspiration, E_0 is less than the amount of free water held in the canopy, R_{INT}, then

$$E_{\text{a}} = E_{\text{can}} = E_0 \tag{A13}$$

$$R_{\text{INT(f)}} = R_{\text{INT(i)}} - E_{\text{can}} \tag{A14}$$

Where E_0 is the actual amount of evapotranspiration occurring in the watershed on a given day (mm H_2O), E_{can} is the amount of evaporation from free water in the canopy on a given day (mm H_2O), E_0 is the potential evapotranspiration on a given day (mm H_2O), $R_{\text{INT(i)}}$ is the initial amount of free water held in the canopy on a given day (mm

HESSD
8, 9005–9062, 2011

H2O), and $R_{INT(f)}$ is the final amount of free water held in the canopy on a given day (mm H_2O). If potential evapotranspiration, E_0, is greater than the amount of free water held in the canopy, R_{INT}, then

$$E_{can} = R_{INT(i)} \quad \text{(A15)}$$

$$R_{INT(f)} = 0 \quad \text{(A16)}$$

Once any free water in the canopy has been evaporated, the remaining evaporative water demand ($E'_0 = E_0 - E_{can}$) is portioned between the vegetation.

A2.2 Transpiration

Transpiration is calculated for the methods of Hargreaves and Priestely Talyor methods of estimating potential evapotranspiration as:

$$E_t = \frac{E'_0 \cdot LAI}{3.0} \quad \text{(A17)}$$

$$E_t = E'_0 \quad \text{(A18)}$$

Where E_t is the maximum transpiration on a given day (mm H_2O), E'_0 is the potential evapotranspiration adjusted for evaporation of free water in the canopy (mm H_2O), and LAI is the leaf area index. The value for transpiration calculated by Eqs. (A17) and (A18) is the amount of transpiration that will occur on a given day when the plant is growing under ideal conditions. The actual amount of transpiration may be less than this due to lack of available water in the soil profile.

A2.3 Sublimation and evaporation from the soil

The amount of sublimation and soil evaporation will be impacted by the degree of shading. The maximum amount of sublimation/evaporation on a given day is calculated as:

$$E_s = E'_0 \cdot cov_{sol} \quad \text{(A19)}$$

HESSD
8, 9005–9062, 2011

Where E_s is the maximum sublimation/evaporation on a given day (mm H_2O), E_0' is the potential evapotranspiration adjusted for evaporation of free water in the canopy (mm H_2O), and cov_{sol} is the soil cover index. The soil cover index is calculated

$$cov_{sol} = \exp\left(-5.0 \times 10^{-5} CV\right) \quad \text{(A20)}$$

Where CV is the above ground biomass and residue (kg ha^{-1}). If the snow water conent is greater than 0.5 mm H_2O, the soil cover index is set to 0.5.

The maximum amount of sublimation/soil evaporation is reduced during periods of high plant water use with the relationship;

$$E_s' = \min\left[E_s' \frac{E_s E_0'}{E_s + E_t}\right] \quad \text{(A21)}$$

Where E_s' is the maximum sublimation/soil evaporation adjusted for plant water use on a given day (mm H_2O), E_s is the maximum sublimation/soil evaporation on a given day (mm H_2O), E_0' is the potential evapotranspiration adjusted for evaporation of free water in the canopy (mm H_2O), and E_t is the transpiration on a given day (mm H_2O). When E_t is low $E_s' \rightarrow E_s$ However, as E_t approach E_0',

$$E_s' \rightarrow \frac{E_s}{1 + cov_{sol}} \quad \text{(A22)}$$

A2.4 Sublimation

Once the maximum amount of sublimation/soil evaporation for the day is calculated, SWAT will first remove water from the snow pack to meet the evaporative demand. If the water content of the snowpack is greater than the maximum sublimation/soil evaporation demand, then

$$E_{sub} = E_s' \quad \text{(A23)}$$

$$SNO_{(f)} = SNO_{(i)} - E_s' \quad \text{(A24)}$$

$$E_s'' = 0 \quad \text{(A25)}$$

HESSD
8, 9005–9062, 2011

Where E_{sub} is the amount of sublimation on a given day (mm H_2O), E'_s is the maximum sublimation/soil evaporation adjusted for plant water use on a given day prior to accounting for sublimation (mm H_2O), $SNO_{(i)}$ is the amount of water in the snow pack on a given day prior to accounting for sublimation (mm H_2O), $SNO_{(f)}$ is the amount of water in the snow pack on a given day after accounting for sublimation (mm H_2O), and E''_s is the maximum soil water evaporation on a given day (mm H_2O). If the water conent of the snowpack is less than the maximum sublimation/soil evaporation demand, then

$$E_{sub} = SNO_{(i)} \tag{A26}$$

$$SNO_{(f)} = 0, \tag{A27}$$

$$E''_s = E'_s - E_{sub} \tag{A28}$$

A2.5 Soil water evaporation

When an evaporation demand for soil water exists, SWAT must first partition the evaporation demand between the different layers. The depth distribution used to determine the maximum amount of water allowed to be evaporated is:

$$E_{soil,z} = E''_s \frac{z}{z + \exp(2.374 - 0.00713z)} \tag{A29}$$

Where $E_{soil,z}$ is the evaporative demand at depth z (mm H_2O), E''_s is the maximum soil water evaporative on a given day (mm H_2O), and z is the depth below the surface.

A2.6 Percolation

Percolation is the downward movement of water through the soil. In SWAT, percolation is calculated for each soil layer in the profile. The percolation component of SWAT uses a storage routing technique to predict flow through each soil layer in the root

HESSD
8, 9005–9062, 2011

zone. Water is allowed to percolate if the water content exceeds the field capacity water content for that layer. The downward flow rate is governed by the saturated hydraulic conductivity of the soil layer. Upward flow may occur when a lower layer exceeds field capacity. The soil water to field capacity ratios of the two layers regulates movement from a lower layer to an adjoining upper layer. Percolation is also affected by soil temperature. Percolation will not allow in the soil at a particular layer, if the temperature in the layer is 0 °C or below.

The volume of water available for percolation in the soil layer is calculated:

$$SW_{ly,excess} = SW_{ly} - FC_{ly} \quad \text{if} \quad SW_{ly} > FC_{ly} \tag{A30}$$

$$SW_{ly,excess} = 0 \quad \text{if} \quad SW_{ly} \leq FC_{ly} \tag{A31}$$

where $SW_{ly,excess}$ is the drainable volume of water in the soil layer on a given day (mm of water), SW_{ly} is the water content of the soil layer on a given day (mm of water) and FC_{ly} is the water content of the soil layer at field capacity (mm of water).

The amount of water that moves from one layer to the underlying layer is calculated using storage routing methodology. The equation used to calculate the amount of water that percolates to the next layer is:

$$w_{perc,ly} = SW_{ly,excess} \cdot \left(1 - \exp\left[\frac{-\Delta t}{TT_{perc}}\right]\right) \tag{A32}$$

where $w_{perc,ly}$ is the amount of water percolating to the underlying soil layer on a given day (mm of water), $SW_{ly,excess}$ is the drainable volume of water in the soil layer on a given day (mm of water), Δt is the length of the time step (h), and TT_{perc} is the travel time for percolation (h).

The total amount of water exiting the bottom of the soil profile on day i is calculated:

$$w_{seep} = w_{perc,ly=n} + w_{crk,btm} \tag{A33}$$

where w_{seep} is the total amount of water exiting the bottom of the soil profile on day i (mm), $w_{perc,ly=n}$ is the amount of water percolating out of the lowest layer, n, in the soil

HESSD
8, 9005–9062, 2011

profile on day i (mm), and $w_{crk,btm}$ is the amount of water flow past the lower boundary of the soil profile due to bypass flow on day i (mm).

A2.7 Groundwater flow

Groundwater balance in SWAT model is calculated by assuming two layers of aquifers. SWAT partitions groundwater into a shallow, unconfined aquifer and a deep-confined aquifer and it simulates two aquifers in each subbasin. The shallow aquifer is an unconfined aquifer that contributes to flow in the main channel or reach of the subbasin. The deep aquifer is a confined aquifer. Water that enters the deep aquifer is assumed to contribute to streamflow somewhere outside of the watershed (Arnold et al., 1993).

Groundwater flow contribution to total streamflow is simulated by creating shallow aquifer storage (Arnold et al., 1993). Percolate from the bottom of the root zone is recharge to the shallow aquifer. A recession constant, derived from daily streamflow records, is used to lag flow from the aquifer to the stream.

The water balance for a shallow aquifer in SWAT is calculated with:

$$aq_{sh,i} = aq_{sh,i-1} + w_{rchrg} - Q_{gw} - w_{revap} - w_{deep} - w_{pump,sh} \quad \text{(A34)}$$

where $aq_{sh,i}$ is the amount of water stored in the shallow aquifer on day i (mm), $aq_{sh,i-1}$ is the amount of water stored in the shallow aquifer on day $i-1$ (mm), w_{rchrg} is the amount of recharge entering the aquifer on day i (mm), Q_{gw} is the groundwater flow, or base flow, into the main channel on day i (mm), w_{revap} is the amount of water moving into the soil zone in response to water deficiencies on day i (mm), w_{deep} is the amount of water percolating from the shallow aquifer into the deep aquifer on day i (mm), and $w_{pump,sh}$ is the amount of water removed from the shallow aquifer by pumping on day i (mm).

The shallow aquifer contributes base flow to the main channel or reaches within the subbasin. Base flow is allowed to enter the reach only if the amount of water stored in the shallow aquifer exceeds a threshold specified by the user, $aq_{shthr,q}$.

HESSD
8, 9005–9062, 2011

The steady-state response of groundwater flow to recharge is (Hooghoudt, 1940):

$$Q_{gw} = \frac{800 K_{sat}}{L_{gw}^2} h_{wtbl} \quad \text{(A35)}$$

where Q_{gw} is the groundwater flow, or base flow, into the main channel on day i (mm), K_{sat} is the hydraulic conductivity of the aquifer (mm day^{-1}), L_{gw} is the distance from the ridge or subbasin divide for the groundwater system to the main channel (m), and h_{wtbl} is the water table height (m). A water table fluctuation due to non-steady-state response of groundwater flow to periodic recharge is calculated (Smedema and Rycroft, 1983):

$$\frac{dh_{wtbl}}{dt} = \frac{w_{rchrg} - Q_{gw}}{800\mu} \quad \text{(A36)}$$

where $\frac{dh_{wtbl}}{dt}$ is the change in water table height with time (mm day^{-1}), w_{rchrg} is the amount of recharge entering the aquifer on day i (mm), Q_{gw} is the groundwater flow into the main channel on day i (mm), and μ is the specific yield of the shallow aquifer (m m^{-1}).

Assuming that variation in groundwater flow is linearly related to the rate of change in water table height, Eqs. (A35) and (A36) can be combined to obtain:

$$\frac{dQ_{gw}}{dt} = 10\frac{K_{sat}}{\mu L_{gw}^2}\left(w_{rchrg} - Q_{gw}\right) = \alpha_{gw}\left(w_{rchrg} - Q_{gw}\right) \quad \text{(A37)}$$

where Q_{gw} is the groundwater flow into the main channel on day i (mm), K_{sat} is the hydraulic conductivity of the aquifer (mm day^{-1}), μ is the specific yield of the shallow aquifer (m m^{-1}), L_{gw} is the distance from the ridge or subbasin divide for the groundwater system to the main channel (m), w_{rchrg} is the amount of recharge entering the aquifer on day i (mm) and α_{gw} is the base flow recession constant or constant of proportionality. Integration of Eq. (A37) and rearranging to solve for Q_{gw} yields:

$$Q_{gw,i} = Q_{gw,i-1} \cdot \exp\left[-\alpha_{gw} \cdot \Delta t\right] + w_{rchrg} \cdot \left(1 - \exp\left[-\alpha_{gw} \cdot \Delta t\right]\right) \quad \text{(A38)}$$

HESSD
8, 9005–9062, 2011

where $Q_{gw,i}$ is the groundwater flow into the main channel on day i (mm), $Q_{gw,i-1}$ is the groundwater flow into the main channel on day $i-1$ (mm), α_{gw} is the base flow recession constant Δt is the time step (1 day), and w_{rchrg} is the amount of recharge entering the aquifer on day i (mm). The base flow recession constant, α_{gw}, is a direct index of groundwater flow response to changes in recharge (Smedema and Rycroft, 1983). Values vary from 0.1–0.3 for land with slow response to recharge to 0.9–1.0 for land with a rapid response. Although the base flow recession constant may be calculated, the best estimates are obtained by analyzing measured streamflow during periods of no recharge in the watershed.

When the shallow aquifer receives no recharge, Eq. (A38) simplifies to:

$$Q_{gw} = Q_{gw,0} \cdot \exp\left[-\alpha_{gw} \cdot t\right] \tag{A39}$$

where Q_{gw} is the groundwater flow into the main channel at time t (mm), $Q_{gw,0}$ is the groundwater flow into the main channel at the beginning of the recession (time $t = 0$) (mm), α_{gw} is the base flow recession constant, and t is the time lapsed since the beginning of the recession (days). The base flow recession constant is measured by rearranging Eq. (A39).

$$\alpha_{gw} = \frac{1}{N} \ln\left[\frac{Q_{gw,N}}{Q_{gw,0}}\right] \tag{A40}$$

where α_{gw} is the base flow recession constant, N is the time lapsed since the start of the recession (days), $Q_{gw,N}$ is the groundwater flow on day N (mm), $Q_{gw,0}$ is the groundwater flow at the start of the recession (mm). It is common in some areas to find the base flow days reported for a stream gage or watershed. This is the number of days for base flow recession to decline through one log cycle. When base flow days are used, Eq. (A40) can be further simplified:

$$\alpha_{gw} = \frac{1}{N} \cdot \ln\left[\frac{Q_{gw,N}}{Q_{gw,0}}\right] = \frac{1}{\mathrm{BFD}} \cdot \ln[10] = \frac{2.3}{\mathrm{BFD}} \tag{A41}$$

HESSD
8, 9005–9062, 2011

where α_{gw} is the base flow recession constant, and BFD is the number of base flow days for the watershed.

A fraction of the total daily recharge can be routed to the deep aquifer. Percolation to the deep aquifer is allowed to occur only if the amount of water stored in the shallow aquifer exceeds a threshold value specified by the user, $aq_{shthr,rvp}$.

The maximum amount of water then will be removed from the shallow aquifer via percolation to the deep aquifer on a given day is:

$$w_{deep,mx} = \beta_{deep} w_{rchrg} \tag{A42}$$

where $w_{deep,mx}$ is the maximum amount of water moving into the deep aquifer on day i (mm), β_{deep} is the aquifer percolation coefficient, and w_{rchrg} is the amount of recharge entering the aquifer on day i (mm). The actual amount of percolation to the deep aquifer that will occur on a given day is calculated:

$$w_{deep} = 0 \quad \text{if} \quad aq_{sh} \le aq_{shthr,rvp} \tag{A43}$$

$$w_{deep} = w_{deep,mx} - aq_{shthr,rvp} \quad \text{if} \quad aq_{shthr,rvp} < aq_{sh} < \left(aq_{shthr,rvp} + w_{revap,mx}\right) \tag{A44}$$

$$w_{deep} = w_{deep,mx} \quad \text{if} \quad aq_{sh} \ge \left(aq_{shthr,rvp} + w_{revap,mx}\right) \tag{A45}$$

where w_{deep} is the actual amount of water moving into the deep aquifer on day i (mm), $w_{deep,mx}$ is the maximum amount of water moving into the deep aquifer on day i (mm), aq_{sh} is the amount of water stored in the shallow aquifer at the beginning of day i (mm) and $aq_{shthr,rvp}$ is the threshold water level in the shallow aquifer for revap or percolation to deep aquifer to occur (mm).

The water balance for the deep aquifer is:

$$aq_{dp,i} = aq_{dp,i-1} + w_{deep} - w_{pump,dp} \tag{A46}$$

where $aq_{dp,i}$ is the amount of water stored in the deep aquifer on day i (mm), $aq_{dp,i-1}$ is the amount of water stored in the deep aquifer on day $i-1$ (mm), w_{deep} is the amount of water percolating from the shallow aquifer into the deep aquifer on day i (mm), and $w_{pump,dp}$ is the amount of water removed from the deep aquifer by pumping on day i

HESSD
8, 9005–9062, 2011

(mm). If the deep aquifer is specified as the source of irrigation water or water removed for use outside the watershed, the model will allow an amount of water up to the total volume of the deep aquifer to be removed on any given day.

Water entering the deep aquifer is not considered in future water budget calculations and can be considered to be lost from the system.

Appendix B

See Fig. B1.

Acknowledgement. This work has been carried out with support from the Ethiopian Malaria Prediction System (EMaPS) project funded by the Norwegian Programme for Development, Research and Education (NUFU). The authors would like to acknowledge Ministry of Water Resources and National Meteorological Agency of Ethiopia for provision of streamflow and meteorological data of the entire basin. We also appreciate the contribution of Dr. Semu Moges for initiating this project together with other partners.

References

Allen, R. G.: A penman for all seasons, J. Irrigat. Drain Engin. ASCE, 12(4), 348–368, 1986.

Arnold, J. G. and Allen, P. M.: Estimating hydrologic budgets for three Illinois watersheds, J. Hydrol., 176(1–4), 57–77, 1996.

Arnold, J. G., Allen, P. M., and Bernhardt, G.: A comprehensive surface groundwater flow model, J. Hydrol., 142, 47–69, 1993.

Arnold, J. G., Sirinivasan, R., Muttiah, R. S., and Williams, J. R.: Large area hydrologic modelling and assessment, Part 1: Model development, J. Am. Water Resour. Assoc., 7389, 1998.

Arsano, Y.: Ethiopia and the Nile: The Dilemma of National and Regional Hydro-politics, PhD dissertation, Zurich, Switzerland, University of Zurich, 2004.

Arsano, Y.: Ethiopia and the Eastern Nile basin, Aquat. Sci., 67, 16–17, doi:10.1007/s00027-004-0766-x, 2005.

Barrett, C. B.: The development of the Nile hydrometeorological forecast system, Hydrol. Process., 933–938, 1993.

HESSD

8, 9005–9062, 2011

Chiew, F. H. S.: Estimation of rainfall elasticity of streamflow in Australia, Hydrol. Sci. J., 51, 613–625, 2006.
Checkol, D. A.: Modeling of Hydrology and Soil Erosion of Upper Awash River Basin, Cuvillier, Göttingen, 2006.
Conway, D.: A water balance model of the upper Blue Nile in Ethiopia, Hydrol. Sci. J., 42(2), 265–286, 1997.
Duan, Q., Sorooshian, S., and Gupta, V.: Effective and efficient global optimisation for conceptual rainfall-runoff models, Water Resour. Engin., 1015–1031, doi:10.1029/91WR02985, 1992.
Dugale, G., Hardy, S., and Milford, J. R.: Daily catchment rainfall estimated from METEOSAT, Hydrol. Process., 5, 261–270, 1991.
Eckhardt, K. and Arnold, J. G.: Automatic calibration of a distributed catchment model, J. Hydrol., 251, 103–109, 2001.
Elshamy, M. E., Seierstad, I. A., and Sorteberg, A.: Impacts of climate change on Blue Nile flows using bias-corrected GCM scenarios, Hydrol. Earth Syst. Sci., 13, 551–565, doi:10.5194/hess-13-551-2009, 2009.
FAO: Soils of EAST Afica, SEA, Food and Agriculture Organization of the United Nations, A CD-Rom Data, Rome, 1995.
FAO: The Soil and Terrain Database for Northeastern Africa (CD-ROM), FAO, Rome, 1998.
Fu, G., Charles, S. P., and Chiew, F. H. S.: A two-parameter climate elasticity of streamflow index to assess climate change effects on annual streamflow, Water Resour. Res., 43, W11419, doi:10.1029/2007WR005890, 2007.
Gan, T. Y.: Application of scientific modelling of hydrological responses from hypothetical small catchments to access a complex conceptual rainfall runoff model, Water Resources Series Tech. Rept. 111, University of Washington, Seattle, Washington, 1988.
Green, W. H. and Ampt, G. A.: Studies on soil physics. 1. The flow of air and water through soils, J. Agric. Sci., 4, 11–24, 1911.
van Griensven, A., Francos, A., and Bauwens, W.: Sensitivity analysis and auto-calibration of an integral dynamic model for river water quality, Water Sci. Technol., 321–328, 2002.
Guo, H., Hu, Q., and Jiang, T.: Annual and seasonal streamflow responses to climate and land-cover changes in the Poygan Lake basin, China, J. Hydrol., 355, 106–122, 2008.
Hamouda, M. A., Nour El-Din, M. M., and Moursy, F. I.: Vulnerability assessment of water resorces system in the Eastern Nile basin, Water Resources Manage., 23, 2697–2725, 2009.

HESSD
8, 9005–9062, 2011

Hansen, M., Defries, R., Townshend, J. R. G., and Sohlberg, R.: UMD Global Land Cover Classification, Specify 1 Degree, 8 Kilometer, or 1 Kilometer (1.0), Department of Geography, University of Maryland, College Park, Maryland, 1981–1994, 1998.
Hargreaves, G. H. and Samani, Z. A.: Agricultural benefits for Senegal river basin, J. Irrigat. Drain. Engin., 111, 113–124, doi:10.1061/(ASCE)0733-9437(1985)111:2(113) 1985.
Hooghoudt, S. B.: Bijdrage tot de kennis van enige natuurkundige grootheden van de grond, Versl. Landbouwkd. Onderz, 46, 515–707, 1940.
Johanson, P. A. and Curtis, P. D.: Water balance of Blue Nile River basin in Ethiopia, J. Irrigat. Drain. Engin., 120, 573–590, 1994.
Lenhart, T., Eckhardt, K., Fohrer, N., and Frede, H. G.: Comparison of two different approaches of sensitivity analysis, Phys. Chem. Earth, 27, 645–654, 2002.
Mohamed, Y. A., van den Hurk, B. J. J. M., Savenije, H. H. G., and Bastiaanssen, W. G. M.: Hydroclimatology of the Nile: results from a regional climate model, Hydrol. Earth Syst. Sci., 9, 263–278, doi:10.5194/hess-9-263-2005, 2005.
Monteith, J. L.: Evaporation and the Environment. The State and Movement of Water in Living Organisms, Cambridge University Press, Sawnsea, 205–234, 1965.
MoWR: Ethiopian water sector strategy, Ministry of Water Resources, Addis Abeba, 2002.
Neitsch, S. L., Arnold, J. G., Kiniry, J. R., Srinivasan, R., and Williams, J. R.: Soil and Water Assessment Tool User's Manual, Version 2000, Temple, Tx.USDA Agricultural Research Service and Texas A&M Blackland Research Center, 2002a.
Neitsch, S. L., Arnold, J. G., Kiniry, J. R., Srinivasan, R., and Williams, J. R.: Soil and Water Assessment Tool SWAT Theory, Version 2000, Temple, Tx.USDA Agricultural Research Service and Texas A&M Blackland Research Center, 2005.
Nicks, A. D.: Stochastic generation of the occurrence, pattern and location of maximum amount of daily rainfall. Statistical hydrology, US Governmental Print Office, Washington, DC, 154–171, 1974.
Ponce, V. M. and Hawkins, R. H.: Runoff curve number: has it reached maturity?, J. Hydrol. Engin., 1(1), 11–19, 1996.
Ritchie, J. T.: Model for predicting evaporation from a row crop with incomplete cover, Water Resour., 1204–1213, 1972.
Rossi, C. G., Dybala, T. J., Moriasi, D. N., Arnold, J. G., Amonett, C., and Marek, T.: Hydrologic calibration and validation of the soil and water assessment tool for the Leon River watershed, J. Soil Water Conserv., 533–541, 2008.

HESSD
8, 9005–9062, 2011

Samani, H. A.: Reference crop evapotarnspiration from temeperature, Appl. Engin. Agric., 96–99, 1985.
Sankarasubramanian, A., Vogel, R. M., and Limbrunner, J. F.: Climate elasticity of streamflow in the United States, Water Resour. Res., 37, 1771–1781, 2001.
Santhi, C., Arnold, J. G., Williams, J. R., Dugas, W. A., Srinivasan, R., and Hauck, L. M.: Validation of the SWAT Model on large River Basin with point and Nonpoint sources, J. Am. Water Res. Assoc., 37, 1169–1188, 2001.
Schaake, J. C.: GIS structure for the Nile River forecast project, in: Application of Geographic Information Sytems in Hydrology and Water Resources Management, edited by: Kovar, K. and Nachtnebel, H. P., International Assoc. of Hydro. Sc. pub. No. 211, Wallingford, 1993.
Setegen, S. G., Srinivasan, R., and Dargahi, B.: Hydrological modelling in the Lake Tana basin, Ethiopia using SWAT model, Open Hydrol. J., 2, 49–62, 2008.
Smedema, L. K. and Rycroft, D. W.: Land Drainage. Planning and Design of Agricultural Drainage Systems, Cornell Uinersity, New York, 1983.
Sorooshian, S. and Gupta, V. K.: Model calibration, in: Computer Models of Watershed Hydrology, edited by: Singh, V. P., Water Resources Publications, Colorado, USA, 1995.
Sutcliffe, J. V., Dugdale, G., and Milford, J. R.: The Sudan floods of 1988, Hydrol. Sci. J., 31, 355–364, 1989.
Swain, A.: Ethiopia, the Sudan, and Eygpt: the Nile River diispute, J. Mod. African Stud., 35, 675–694, 1997.
Taylor, P. A.: On the assessment of surface heat flux and evaporation using large-scale parameters, Weather, 100, 81–92, doi:10.1175/1520-0493(1972)100<0081:OTAOSH>2.3.co;2 1972.
Todd, M. C., Barrett, E. C., Beaumont, M. J., and Green, J. L.: Satellite identification of rain days over the upper Nile River basin using an optimum infrared rain/no-rain threshold temperature model, J. Appl. Meteor., 34, 2600–2611, doi:10.1175/1520-0450(1995)034<2600:SIORDO>2.0.CO;2, 1995.
USDA: Soil Taxonomy, 2nd edn., US Agriculture, Edn., US Government Printinig Office, Washington, DC, 1999.
USDA-SCS: Hydrology, in: National Engineering Hand Book Sect. 4, Washington, DC, USDA-SCS, 1972.
USDA-SCS: Hydrology (Revised), in: Engineering Handbook Sect. 4, Washington, DC, 1985.
Wambeke: Properties and management of soils of the tropics, FAO Land and Water Digital

HESSD
8, 9005–9062, 2011

Media Series, Rome, 2003.
Williams, J. R.: The EPIC model, in: Computer Models of Watershed Hydrology, Water Resources Publications, Highlands Ranch, CO, 909–1000, 1995.
Zeray, L.: Calibration and Validation of SWAT Hydrologic Model for Meki Watershed, Ethiopia, Conference of International Agricultural Research for Development, University of Kassel-Wizenhausen and University of Gottingen, October 2007.

HESSD
8, 9005–9062, 2011

Table 1. Digital elevation model (DEM), soil and land use data sources of Eastern Nile.

Data type	Resolution	Data descriptions
DEM (Topographical data)	1 km × 1 km	Elevation data from Ethiopia ministry of water resources
Soil	10 km × 10 km	Soil texture data from ministry of water resources supplemented by the FAO soil data base
Land use	1 km × 1 km	Land classification and their attributes from Ethiopia ministry of water resources

HESSD
8, 9005–9062, 2011

Table 2. Meteorological data types, number of stations of the Eastern Nile explored for the model simulation.

Data type	Number of stations	Data descriptions
Temperature (Tmax and Tmin)	– Blue Nile, 42 stations – Baro Akobo, 8 stations – Tekeze, 10 stations	Daily data from the Ethiopian National Meteorological Agency (NMSA)
Precipitation	– Blue Nile 74 stations – Baro Akobo, 12 stations – Tekeze, 11 stations	Daily data from the Ethiopian National Meteorological Agency (NMSA)

HESSD
8, 9005–9062, 2011

Table 3. List of stream gauges, dates for calibration and verification used for model simulation.

Stream gauge	Calibration date[1]	Validation date
Tana outlet (Blue Nile)	1 Jan 1991–31 Dec 1996	1 Jan 1997–31 Dec 2000
Kessie (Blue Nile)	1 Jan 1991–31 Dec 1996	1 Jan 1997–31 Dec 2000
Diem (Blue Nile)	1 Jan 1991–31 Dec 1996	1 Jan 1997–31 Dec 2000
Embamadre (Tekeze)	1 Jan 1994–31 Dec 1999	1 Jan 2000–1 Dec 2003
Gambella (Baro Akobo)	1 Jan 1990–31 Dec 1998	1 Jan 1999–31 Dec 2004
Pilog (Baro Akobo)	1 Jan 1990–31 Dec 1998	No recorded data

[1] Time period variation were due to differences in readily available measured flow data records.

HESSD
8, 9005–9062, 2011

Table 4. Calibrated values of adjusted parameters for flow calibration of the SWAT 2005 model for Eastern Nile basin.

ID	Parameter	Description	Range[1]	Initial values	Calibrated values		
					Blue Nile	Baro	Tekeze
1	CN_2	Initial SCS CN II value	±25 %	*	−10 %	−12 %	−24 %
2	Sol_K	Saturated hydraulic conductivity [mm/mm]	±25 %	**	−4 %	1.3 %	19 %
3	ESCO	Soil evaporation compensation factor	0.0–1.0	0.95	0.7	0.58	0.8
4	SOL_AWC	Available water capacity [mm water/mm soil]	±25 %	**	+25 %	7 %	9.4 %
5	SOL_Z	Soil depth [mm]	±25 %	**	−4 %	25 %	13 %
6	GWQMN	Threshold water depth in the shallow aquifer for flow [mm]	0.0–5000	0.0	200	319	53
7	CANMX	Maximum canopy storage	0–10	0.0	9.7	2.4	0.31
8	ALPHA_BF	Base flow alpha factor	0.0–1.0	0.048	0.048	0.018	0.002

[1] The ranges are based primarily on recommendations given in the *SWAT User's Manual* (Neitsch et al., 2002a).
* SWAT default parameters and SWAT driven parameters were used.
** Field measured and from literature collected parameters.

HESSD
8, 9005–9062, 2011

Table 5. General reported ratings for Nash–Sutcliffe efficiency (ENS), mean relative bias (PBIAS), root mean square error-standard deviation (RSR) and coefficient of determination (R^2) for calibration and verification processes (adopted from Rossi et al., 2008).

Formulae	Value	Rating
$E_{NS} = 1 - \left[\frac{\sum_{i=1}^{n}(x_{obs}(i) - y_{model}(i))^2}{\sum_{i=1}^{n}(x_{obs}(i) - \overline{x_{obs}})^2}\right]$	> 0.65 0.54–0.65 > 0.50	Very good Adequate Satisfactory
$PBIAS = \left[\frac{\sum_{i=1}^{n}(x_{obs}(i) - y_{model}(i))}{\sum_{i=1}^{n}(x_{obs}(i))} \cdot 100\right]$	$< \pm 20\,\%$ $\pm 20\,\%$ to $40\,\%$ $< \pm 40\,\%$	Good Satisfactory Unsatisfactory
$RSR = \frac{\left[\sqrt{\sum_{i=1}^{n}(x_{obs}(i) - y_{model}(i))^2}\right]}{\sqrt{\sum_{i=1}^{n}(x_{obs}(i) - \overline{x_{obs}})^2}}$	$0.0 \le RSR \le 0.5$ $0.5 < RSR \le 0.6$ $0.6 < RSR \le 0.7$ $RSR \ge 0.70$	Very good Good Satisfactory Unsatisfactory
$R^2 = \frac{\left[\sum_{i}^{n}(x_{obs}(i) - \overline{x}_{obs})(y_{model}(i) - \overline{y}_{model})\right]^2}{\sum_{i}^{n}(x_{obs}(i) - \overline{x}_{obs})^2 \sum_{i}^{n}(y_{model}(i) - \overline{y}_{model})^2}$	≥ 0.6	Satisfactory

HESSD
8, 9005–9062, 2011

Table 6. Summary of daily streamflow statistics for calibration and validation simulation for the Eastern Nile subbasin: dates for calibration and verification period given in Table 3.

Location	Calibration				Validation			
	ENS	RSR	PBIAS	R^2	ENS	RSR	PBIAS	R^2
Tana outlet (Blue Nile)	0.65	0.48	38	0.77	0.55	0.74	25	0.78
Kessie (Blue Nile)	0.62	0.57	14.2	0.77	0.57	0.66	9.9	0.71
Embamadre (Tekeze)	0.50	0.74	20	0.60	0.8	0.60	6.9	0.68
Gambella (Baro AKobo)	0.70	0.45	−10.9	0.65	0.64	0.40	−25.0	0.79
Gilo (Baro Akobo)	0.81	0.46	−11.1	0.86				

HESSD
8, 9005–9062, 2011

Table 7. Summary of monthly steamflow statistics for calibration and validation for the Eastern Nile subbasin dates for calibration and verification period given in Table 3.

Location	Calibration				Validation			
	ENS	RSR	PBIAS	R^2	ENS	RSR	PBIAS	R^2
Tana outlet (Blue Nile)	0.85	0.32	7.2	0.90	0.53	0.71	21	0.86
Kessie (Blue Nile)	0.62	0.58	28	0.90	0.54	0.80	37	0.86
Diem (Blue Nile)	0.90	0.31	−11.3	0.97	0.65	0.39	8.2	0.92
Embamadre (Tekeze)	0.80	0.45	2.2	0.81	0.83	0.42	−13.9	0.88
Gambella (Baro AKobo)	0.90	0.31	−3.8	0.92	0.81	0.44	−23.0	0.89
Gilo (Baro Akobo)	0.93	0.40	−2.4	0.91				

HESSD
8, 9005–9062, 2011

Table 8. Annual averaged calibrated/validated hydrological balances and percent contribution of water balance components for the Eastern Nile basin [I]SURQ: surface runoff, [II]LATQ: lateral flow into stream, [III]GW_Q: groundwater in the shallow aquifer, [IV]ET: evapotanspiration, [V]PET: potential evapotranspiration (Hargreaves method is used), [VI]PERC: percolation below root zone (groundwater recharge), [VII]TLOS: transmission losses.

Subbasin	Period	Rainfall (mm)	SURQ[I] (mm)	LATQ[II] (mm)	GW_Q[III] (mm)	ET[IV] (mm)	PET[V] (mm)	PERC[VI] (mm)	TLOS[VII] (mm)
Blue Nile	Calibration/validation	1422/1547	314.4/410	1.63/1.7	264.8/302	820.9/816	1585/1558	286/327	11/12
	%	100/100	22/26	0.1/0.1	19/20	58/57		20/21	0.8/0.8
Baro Akobo	Calibration/validation	1774/1682	527/492	0.3/0.24	233/199	997/979	1519/1542	253/215	24/23
	%	100/100	30/29	0.2/0.1	13/12	56/58		14/13	1/1
Tekeze	Calibration/validation	931/872	169/162	1.3/1.0	164/140	579/556	1396/1419	179/154	5/4
	%	100/100	18/19	0.1/0.1	18/16	62/64		19/18	0.5/0.5

HESSD
8, 9005–9062, 2011

Table 9. Percentage change in simulated average annual streamflow for each climate scenario compared with the baseline run.

	Precipitation change (%)																			
Temp.	Blue Nile							Baro Akobo							Tekeze					
change	−20	−10	−5	0	5	10	20	−20	−10	−5	0	5	10	20	−20	−10	−5	0	5	10	20
0	−34.9	−18.2	−9.3	0.0	9.8	19.6	40.3	−37.6	−22.5	−14.6	0.0	2.2	10.9	28.9	−42.1	−19.9	−10.8	0.0	12.6	33.0	62.7
+2	−38.6	−22.3	−13.5	−4.4	5.2	14.9	35.4	−43.0	−28.4	−20.6	−6.4	−5.3	4.2	21.8	−41.4	−19.1	−9.5	1.3	13.9	33.8	63.5
+4	−40.4	−24.4	−15.7	−6.6	2.9	12.5	32.8	−43.5	−29.1	−21.4	−7.3	−4.3	3.3	20.8	−44.9	−23.5	−14.0	−3.4	8.8	27.9	57.0

HESSD
8, 9005–9062, 2011

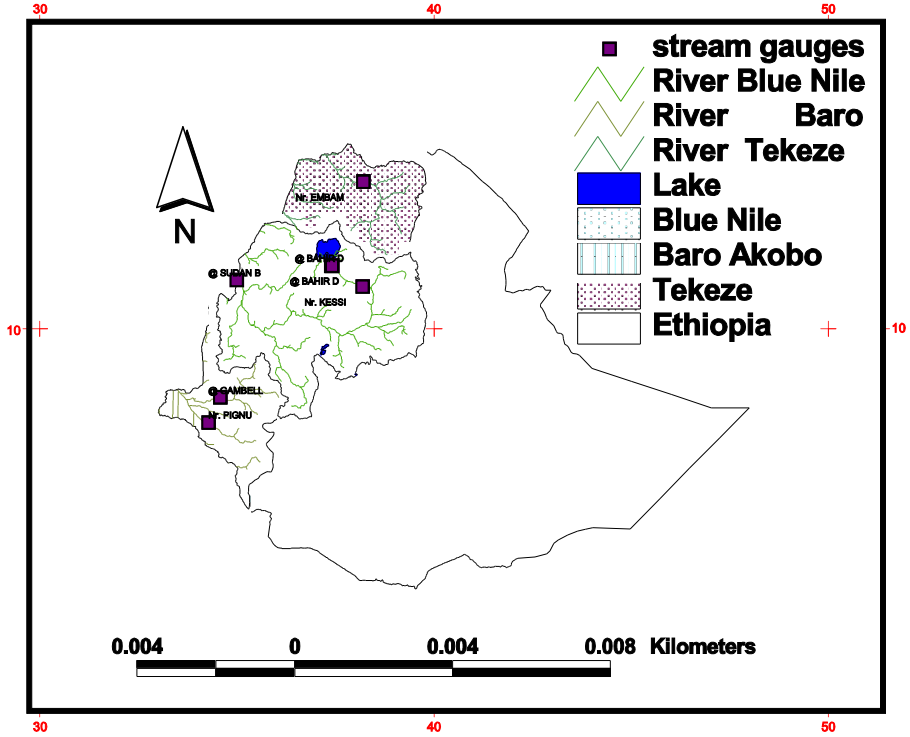

Fig. 1. Water sources of Eastern Nile including stream gauges used for calibration and verification of the model.

HESSD
8, 9005–9062, 2011

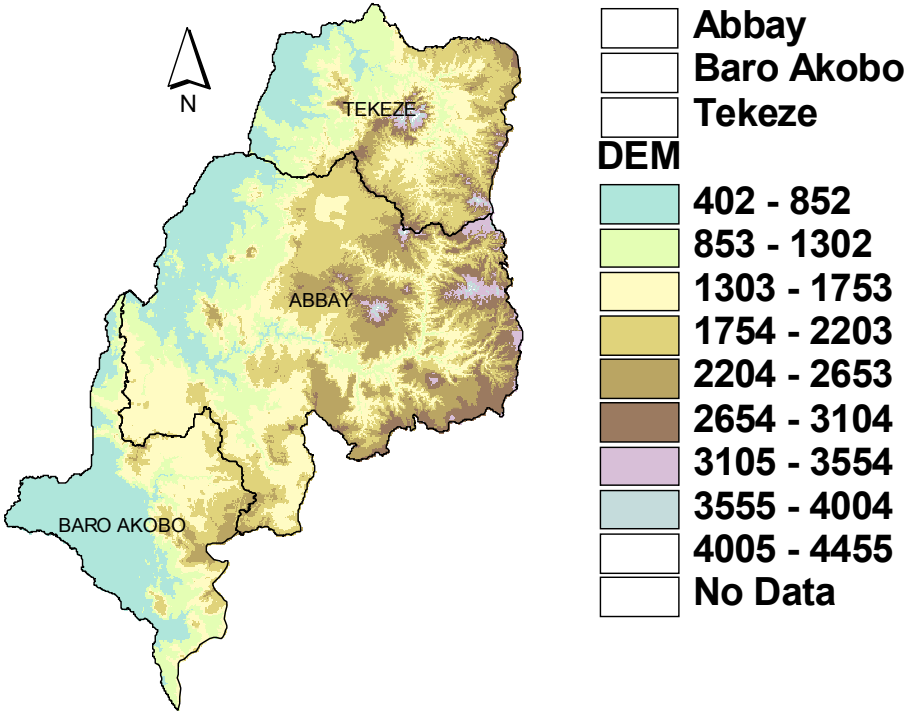

Fig. 2. DEM map of the study area.

HESSD
8, 9005–9062, 2011

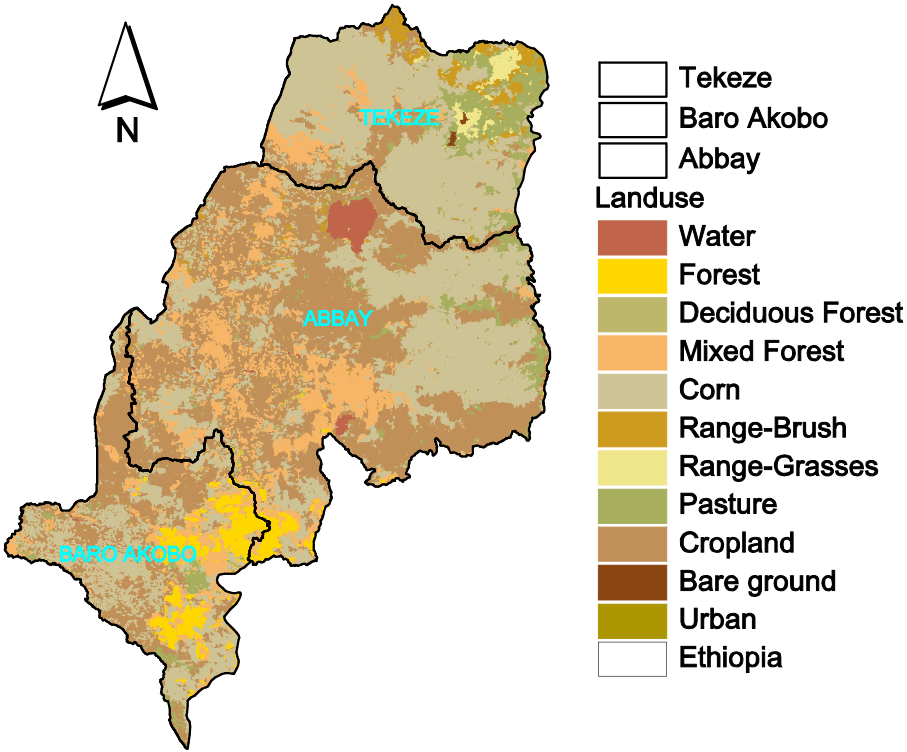

Fig. 3. Map of land uses of the three subbasins.

HESSD
8, 9005–9062, 2011

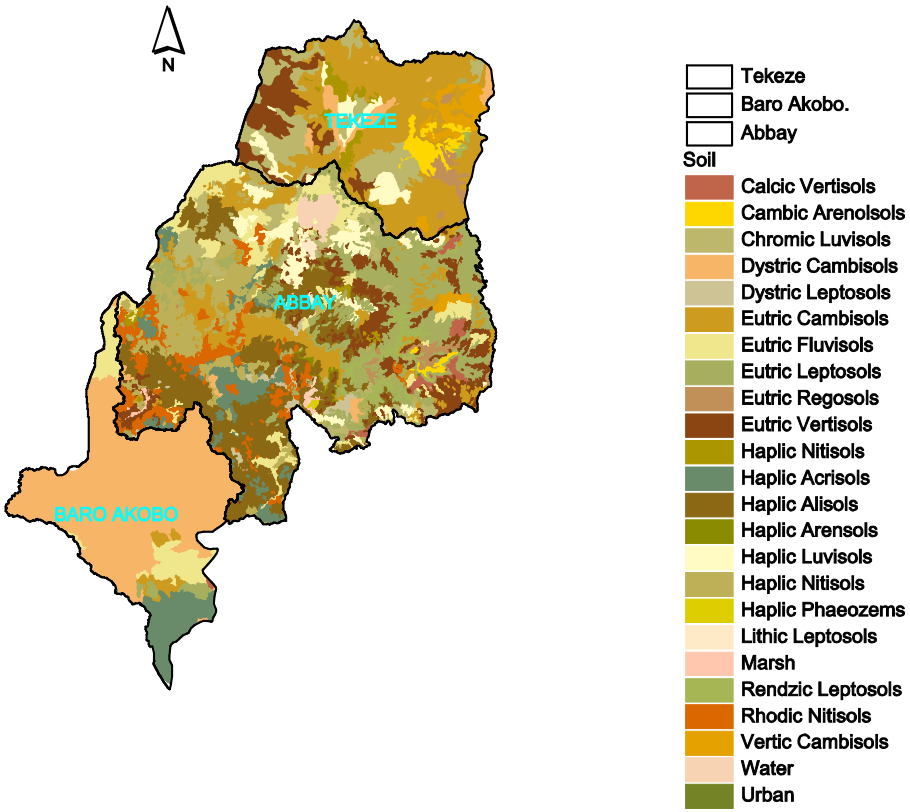

Fig. 4. Map of soil of the three subbasins.

HESSD
8, 9005–9062, 2011

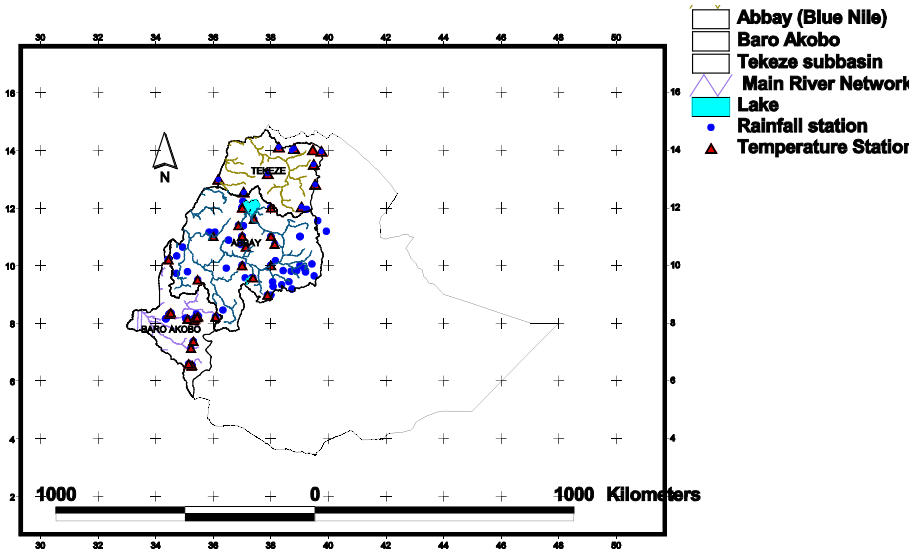

Fig. 5. Meteorological stations distribution of the three subbasins used for the model simulation.

HESSD
8, 9005–9062, 2011

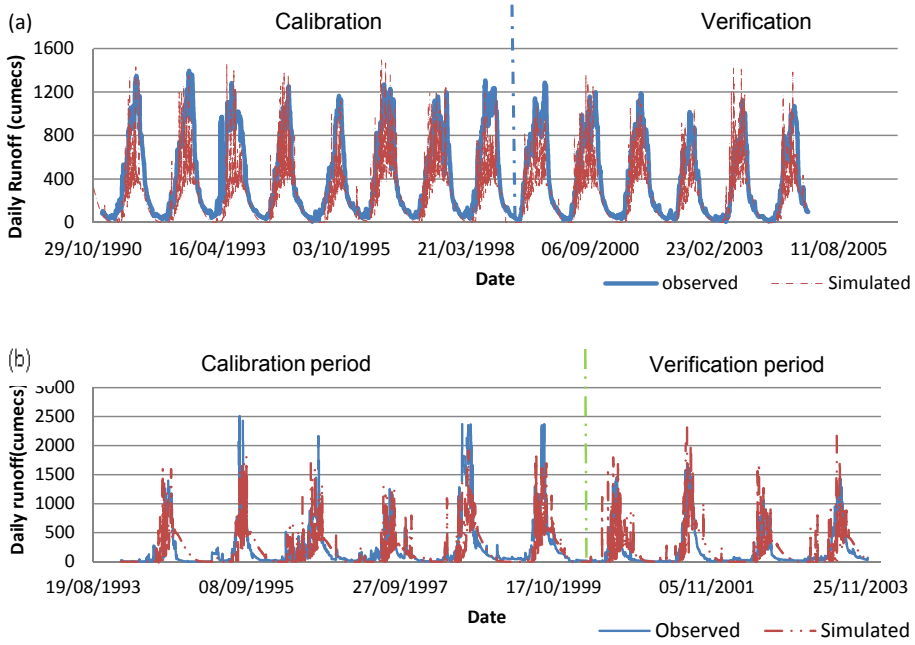

Fig. 6. Daily calibration and verification **(a)** Baro Akobo at Gambella **(b)** Tekeze at Embamadre subbasins.

HESSD
8, 9005–9062, 2011

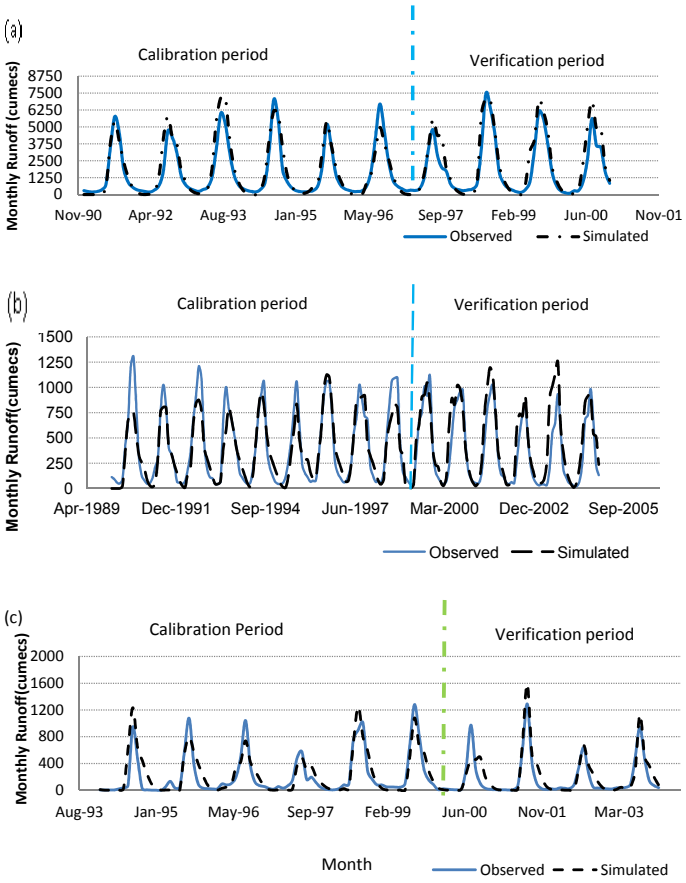

Fig. 7. Monthly calibrations and verifications at **(a)** Diem (Blue Nile), **(b)** Gambella (Baro Akobo) and **(c)** Embamadre (Tekeze) subbasins.

HESSD
8, 9005–9062, 2011

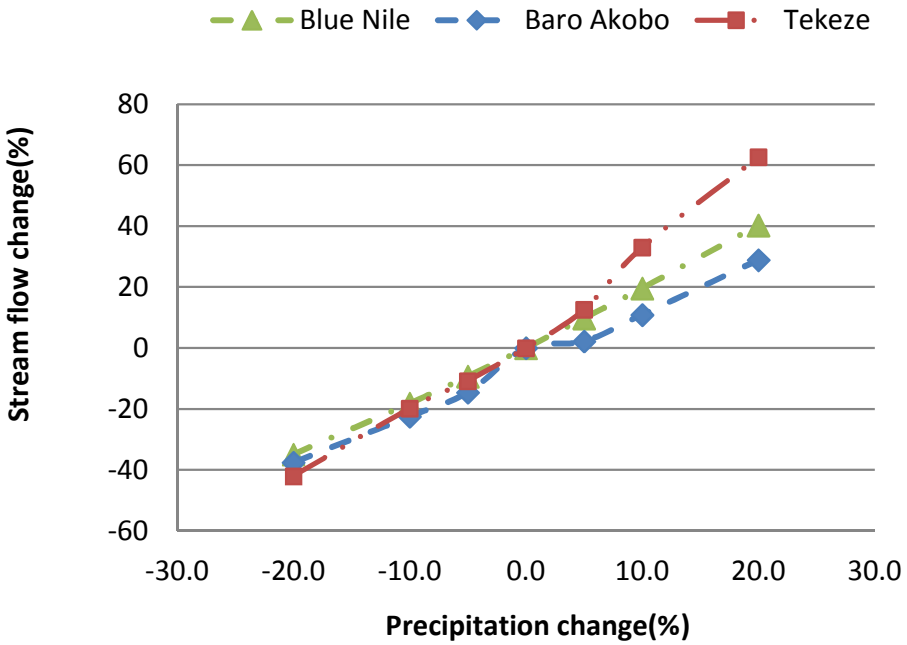

Fig. 8. Annual streamflow changes to precipitation change holding temperature fixed for the three basins.

HESSD
8, 9005–9062, 2011

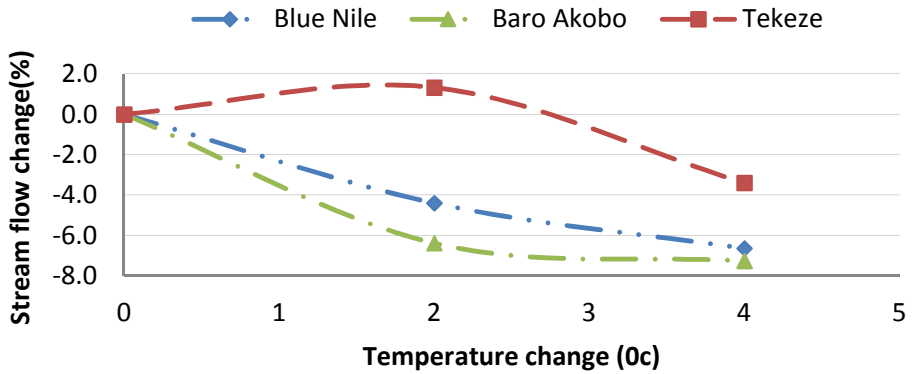

Fig. 9. Annual streamflow changes to temperature change holding precipitation fixed for the three basins.

HESSD
8, 9005–9062, 2011

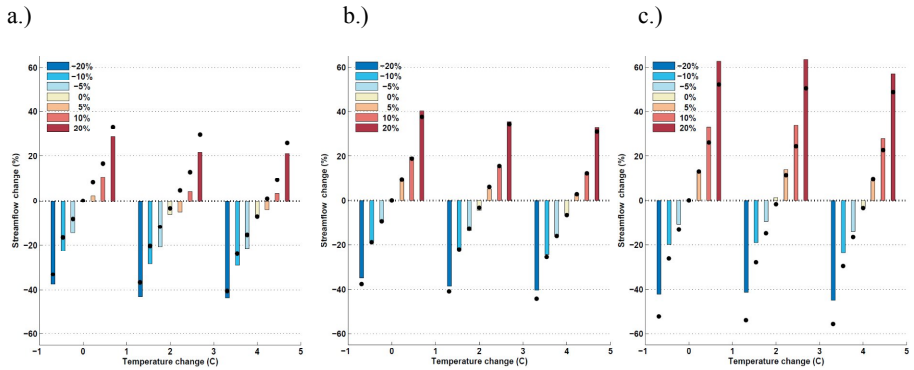

Fig. 10. Change in annual streamflow (%) for different temperature and precipitation scenarios. **(a)** Baro Akobo, **(b)** Blue Nile and **(c)** Tekeze. Black dots indicate the linear sensitivity estimate based on Eq. (3).

HESSD
8, 9005–9062, 2011

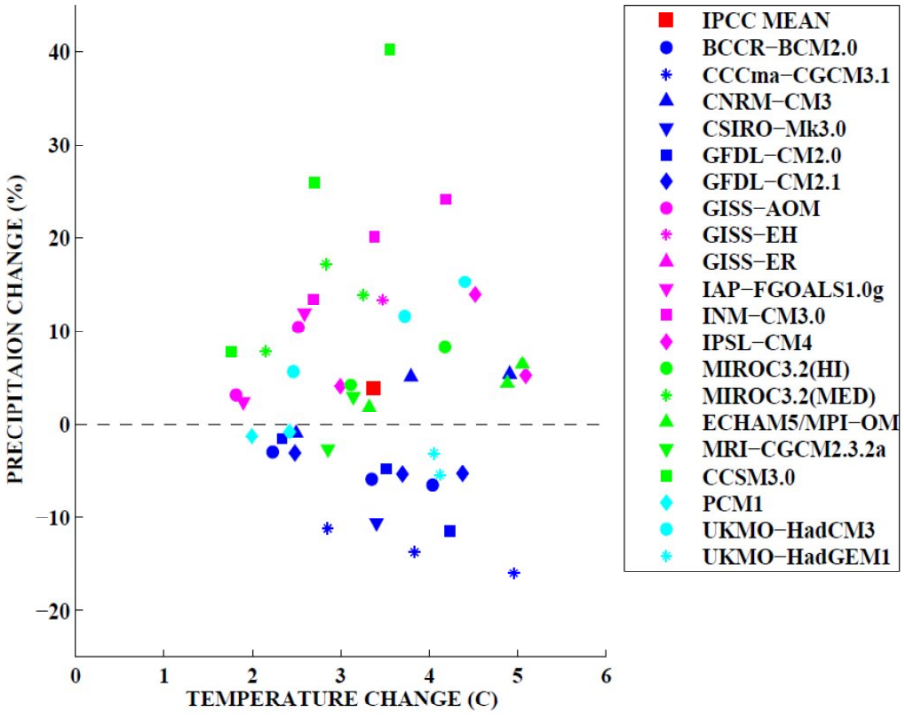

Fig. 11. Change in temperature (˚C) and precipitation (%) for the period 2081–2100 compared to 1981–2000 from 19 AOGCMs and three emission scenarios (totally 47 simulations). Red square indicates the mean change over all simulations.

HESSD
8, 9005–9062, 2011

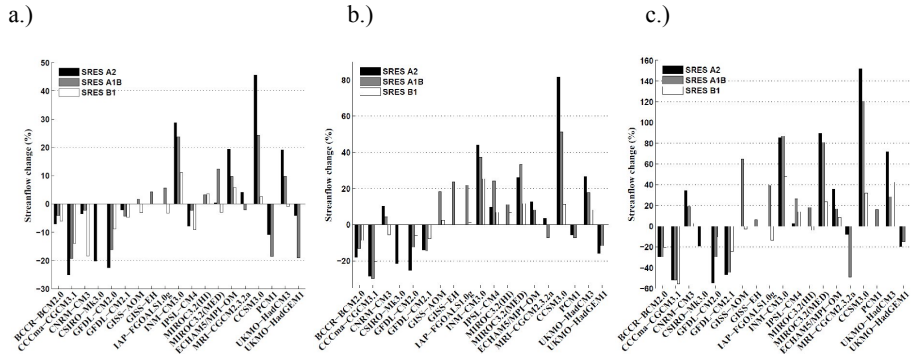

Fig. 12. Change in annual streamflow (%) for **(a)** Baro Akobo, **(b)** Blue Nile and **(c)** Tekeze using the calculated combined temperature-precipitation sensitivities and precipitation and temperature changes (2081–2100 compared to 1981–2000) from 19 AOGCMs and three emission scenarios (totally 47 simulations for each subbasin).

HESSD
8, 9005–9062, 2011

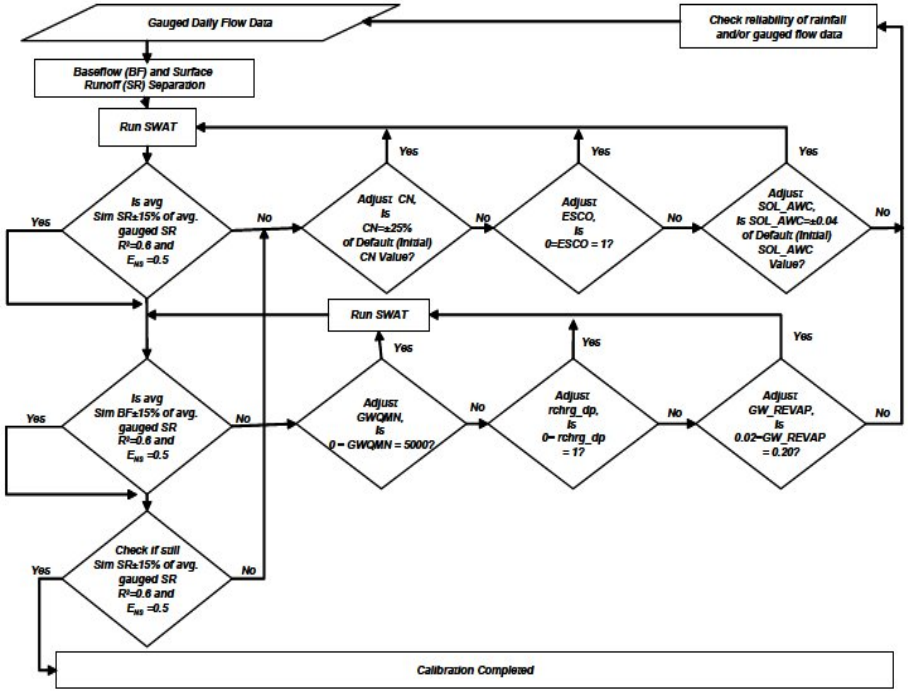

Fig. B1. The manual flow calibration procedure used in this study (adopted from Santhi et al.,2001).

HESSD
8, 9005–9062, 2011